

Functional Versatility of a Series of Zr Metal–Organic Frameworks Probed by Solid-State Photoluminescence Spectroscopy

Ross J. Marshall,[†] Yaroslav Kalinovsky,[‡] Sarah L. Griffin,[†] Claire Wilson,[†] Barry A. Blight,^{*,‡,§} and Ross S. Forgan^{*,†}

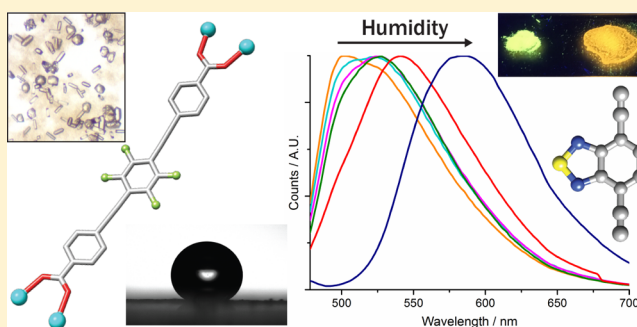
[†]WestCHEM, School of Chemistry, University of Glasgow, University Avenue, Glasgow G12 8QQ, U.K.

[‡]School of Physical Sciences, University of Kent, Ingram Building, Canterbury CT2 7NH, U.K.

[§]Department of Chemistry, University of New Brunswick, Toole Hall, Fredericton, NB E3B 5A3, Canada

Supporting Information

ABSTRACT: Many of the desirable properties of metal–organic frameworks (MOFs) can be tuned by chemical functionalization of the organic ligands that connect their metal clusters into multidimensional network solids. When these linker molecules are intrinsically fluorescent, they can pass on this property to the resultant MOF, potentially generating solid-state sensors, as analytes can be bound within their porous interiors. Herein, we report the synthesis of a series of 14 interpenetrated Zr and Hf MOFs linked by functionalized 4,4′-[1,4-phenylene-bis(ethyne-2,1-diyl)]-dibenzoate (peb²⁻) ligands, and we analyze the effect of functional group incorporation on their structures and properties. Addition of methyl, fluoro, naphthyl, and benzothiadiazolyl units does not affect the underlying topology, but induces subtle structural changes, such as ligand rotation, and mediates host–guest interactions. Further, we demonstrate that solid-state photoluminescence spectroscopy can be used to probe these effects. For instance, introduction of naphthyl and benzothiadiazolyl units yields MOFs that can act as stable fluorescent water sensors, a dimethyl modified MOF exhibits a temperature dependent phase change controlled by steric clashes between interpenetrated nets, and a tetrafluorinated analogue is found to be superhydrophobic despite only partial fluorination of its organic backbone. These subtle changes in ligand structure coupled with the consistent framework topology give rise to a series of MOFs with a remarkable range of physical properties that are not observed with the ligands alone.



INTRODUCTION

Metal–organic frameworks (MOFs)^{1–7} are multidimensional network materials containing both inorganic and organic constituents. The diverse choice of organic and inorganic units that can be used to construct MOFs results in a wide variety of structures.^{8–10} The high porosity of MOFs has prompted investigations toward potential applications such as gas capture and storage,^{11–16} catalysis,^{5,17–19} sensing,^{20–22} and drug delivery.^{23–26} Lately, many synthetic efforts toward MOFs have focused on those containing group IV transition metal ions, especially zirconium and hafnium.^{27–32} Zr and Hf MOFs linked by linear dicarboxylate ligands generally adopt the well-documented UiO-66 topology (UiO = Universitetet i Oslo) which contains M₆O₄(OH)₄ clusters (M = Zr or Hf) linked in three dimensions by 12 bridging organic ligands.²⁷ Alternative topologies of Zr and Hf MOFs have been obtained, usually with nonlinear carboxylate ligands,^{33–37} while extended organic ligands have resulted in interpenetrated UiO-66 analogues.^{38,39} Members of this series of Zr MOFs are constructed from substituted 4,4′-[1,4-phenylene-bis(ethyne-2,1-diyl)]-diben-

zoate (peb²⁻) ligands (Figure 1a) and exhibit a two-fold interpenetrated structure (Figure 1b).³⁸

This family of Zr MOFs has been extended to include an anthracene derivative⁴⁰ and functionalized analogues designed for postsynthetic modification (PSM),⁴¹ while they have been investigated for catalytic applications^{40,42,43} and also CO₂ separation.⁴⁴ We are particularly interested in Zr MOFs containing integral alkyne moieties,⁴⁵ having recently demonstrated their successful postsynthetic halogenation for potential use as I₂ sequestration materials,⁴⁶ and for their ability to modulate the mechanical properties of Zr MOFs, which can be manipulated by the choice of organic ligand.^{47,48}

In 2005, a report detailing the optical properties of the dimethyl ester of the π -conjugated peb²⁻ ligand (L1-Me₂), demonstrated that this ligand precursor exhibited strong absorption in the UV region and was strongly fluorescent, with a quantum yield of 0.91 ($\lambda_{\text{abs}} = 335$ nm) in dichloromethane.⁴⁹ Since then, the Zr MOF containing peb²⁻ (Zr-L1;

Received: March 3, 2017

Published: April 7, 2017

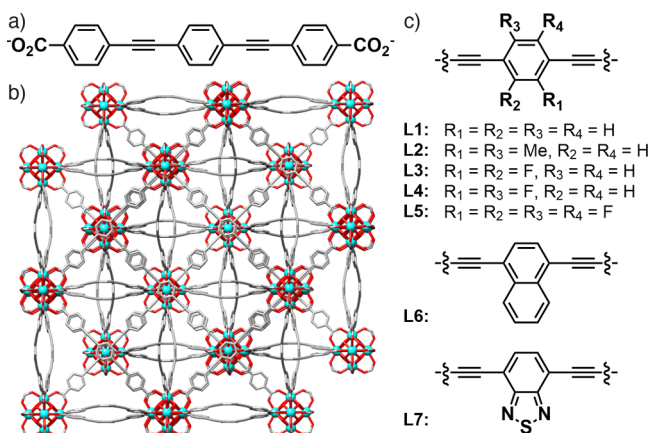


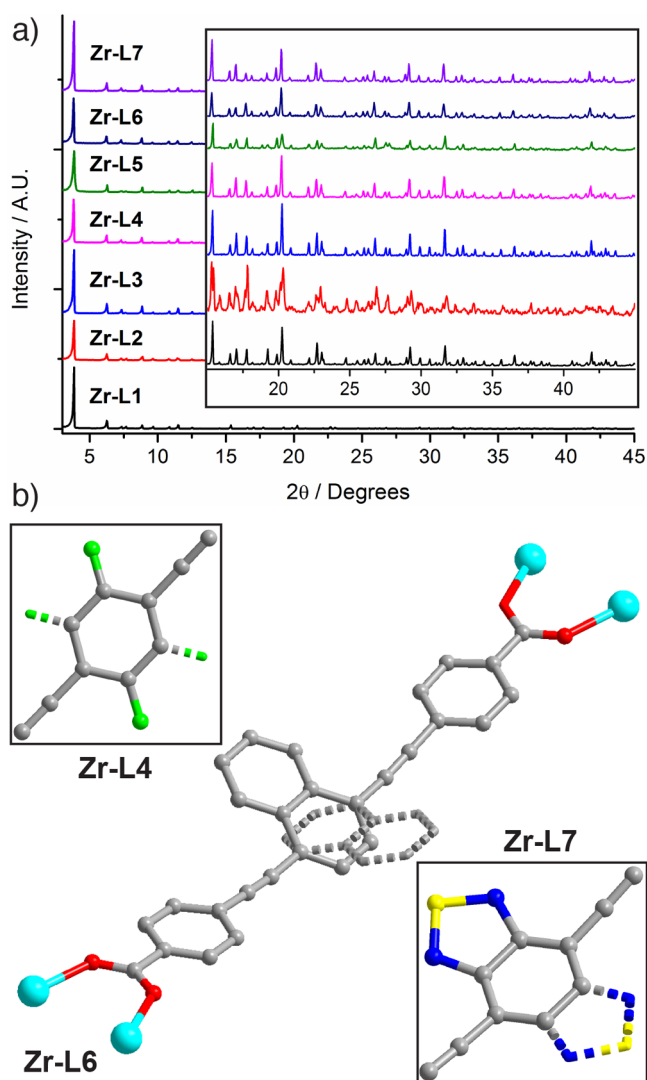
Figure 1b) has been investigated for photocatalytic organic dye degradation; optical measurements and DFT calculations confirmed that the optical properties of the MOF are inherited from the π -conjugated organic ligand.⁴² A number of other fluorescent zirconium MOFs have been reported, and many of them have been used for the detection and sensing of analytes such as metals,⁵⁰ explosives,⁵¹ harmful gases/vapors,^{52–54} and antibiotics.⁵⁵ Alternatively, the intrinsic fluorescence of Zr MOFs has been demonstrated to be useful in pH sensing,^{56,57} while changes in ligand conformation in tetraphenylethylene-⁵⁸ and porphyrin-linked⁵⁹ Zr MOFs have been shown to result in differences in their steady-state emission spectra, in terms of both band positions and intensities.

Inspired by the intrinsic fluorescence of **L1-Me**₂, we herein report the synthesis and structural/optical characterization of a series of interpenetrated Zr and Hf MOFs containing substituted peb^{2-} ligands. We have varied the chemical substituents on the central core of the extended ligand to include methyl, fluorine, naphthyl, and benzothiadiazolyl moieties (Figure 1c). We detail how linker functionalization modulates the structural and optical properties of the resulting Zr and Hf MOFs, whose unusual structural features and host-guest behavior have been probed via solid-state emission techniques.

The dimethyl esters of each of the ligands shown in Figure 1c (see Supporting Information (SI), Scheme S1) were synthesized by Pd/Cu-catalyzed Sonogashira cross-coupling reactions, followed by saponification to produce the free acids (see SI, Section S2). Solvothermal reactions containing the required ligand, ZrCl_4 or HfCl_4 , hydrochloric acid, and either benzoic acid⁶⁰ or L-proline^{61,62} as modulators in DMF resulted in the isolation of a series of new interpenetrated Zr and Hf MOFs (see SI, Section S3). Careful choice of reaction parameters, such as concentration, temperature, and modulator choice/equivalency resulted in the isolation of 14 highly crystalline interpenetrated Zr and Hf MOFs. We described the solid-state structures of $[\text{M}_6\text{O}_4(\text{OH})_4(\text{L1})_6]_n$ ($\text{M} = \text{Zr}$ or Hf) recently⁴⁶ (Figure 1b), and this repeating formula is common to all 14 MOFs. The MOFs are herein described as **M-Ln**, where **M** is

RESULTS AND DISCUSSION

The dimethyl esters of each of the ligands shown in Figure 1c (see Supporting Information (SI), Scheme S1) were synthesized by Pd/Cu-catalyzed Sonogashira cross-coupling reactions, followed by saponification to produce the free acids (see SI, Section S2). Solvothermal reactions containing the required ligand, ZrCl_4 or HfCl_4 , hydrochloric acid, and either benzoic acid⁶⁰ or L-proline^{61,62} as modulators in DMF resulted in the isolation of a series of new interpenetrated Zr and Hf MOFs (see SI, Section S3). Careful choice of reaction parameters, such as concentration, temperature, and modulator choice/equivalency resulted in the isolation of 14 highly crystalline interpenetrated Zr and Hf MOFs. We described the solid-state structures of $[\text{M}_6\text{O}_4(\text{OH})_4(\text{L1})_6]_n$ ($\text{M} = \text{Zr}$ or Hf) recently⁴⁶ (Figure 1b), and this repeating formula is common to all 14 MOFs. The MOFs are herein described as **M-Ln**, where **M** is



either Zr or Hf and **Ln** is the ligand used to construct the framework. Powder X-ray diffraction (PXRD) was used to first analyze the bulk phase purity of the MOFs that were isolated from the synthetic mixtures by centrifugation. Initial attempts at bulk MOF syntheses were performed using our recently discovered L-proline modulation,⁶¹ which proved again to be very efficient. L-Proline effectively modulated 12 of the 14 MOFs; however, it did not produce Zr or Hf MOFs containing the tetrafluoro ligand (**L5**), which is unexpected considering the difluorinated ligands (**L3** and **L4**) were compatible with these synthetic conditions. Instead, we turned to benzoic acid modulation⁶⁰ for **Zr-L5** and **Hf-L5**, and bulk microcrystalline samples were successfully obtained. Upon comparison of the PXRD patterns of the Zr MOFs, it is immediately obvious that all the MOFs are highly crystalline and structurally very similar (Figure 2a),

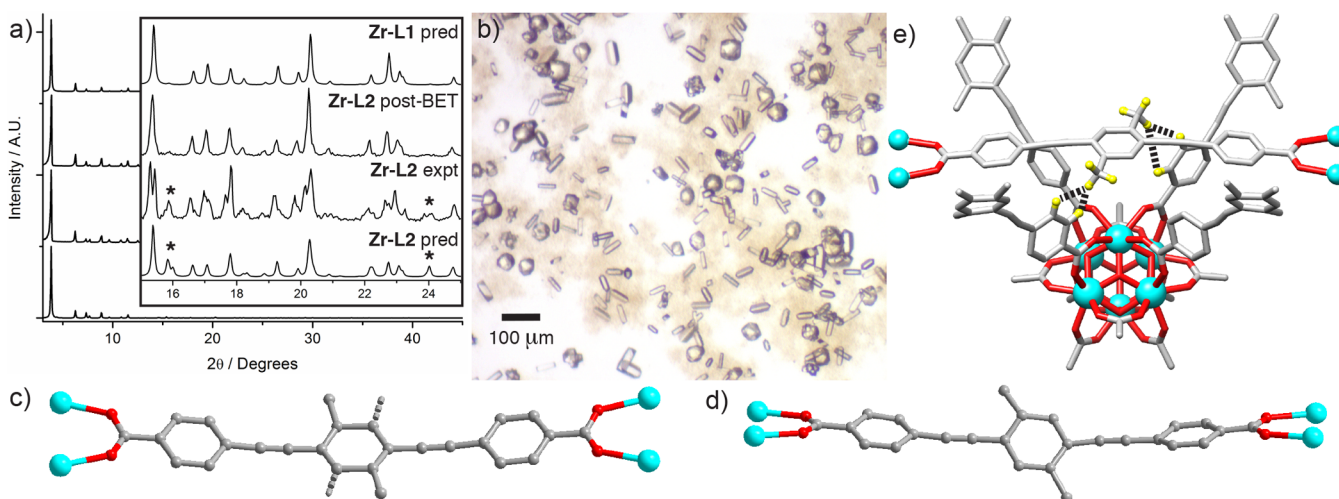


Figure 3. (a) PXRD patterns of Zr-L2 before and after N₂ adsorption measurements compared with predicted patterns of MOFs with orthorhombic and cubic symmetry. Peaks marked with an asterisk are lost on activation, indicating a phase change. (b) Optical microscope image of single crystals of Zr-L2. (c,d) Planar and twisted orientations of L2 observed within Zr-L2, respectively. (e) A portion of the solid-state structure of Zr-L2 (protons and disordered methyl groups have been omitted for clarity) with dashed lines representing the close proximity of the pendant methyl groups with the other framework.

while the Hf MOFs display analogous structures (see SI, Section S4).

Optimization of reaction conditions resulted in the isolation of single crystals of 13 of the MOFs, with Hf-L2 being the only MOF that could not be prepared as diffraction quality single crystals. The crystal structures of the Zr and Hf analogues of individual ligands are very similar, as expected based on the close structural agreement between Zr-L1 and Hf-L1.⁴⁶ The pendant functionality of the ligands does not disrupt formation of the MOFs with all materials displaying two-fold interpenetration. Crystal structures of the Zr and Hf MOFs containing the difluorinated ligands L3 and L4 display positional disorder of the fluorine atoms across all four sites of the central phenylene ring and, on first inspection, they all appear to be identical and resemble the MOFs containing L5. The positional disorder, however, is accounted for by adjusting chemical occupancies (Figure 2b). Similarly, the benzothiazolyl unit of L7 is disordered across two orientations in Zr-L7 and Hf-L7, maintaining the cubic symmetry despite the lower symmetry of the ligand. Interestingly, we observe differences in the solid-state structures of Hf-L6 and Zr-L6, which contain naphthyl units. In Hf-L6 there is similar positional disorder of the naphthyl unit across both sides of the ligand, while in Zr-L6 the same disorder is observed; however, in this case the naphthyl core twists out of the plane of conjugation of the ligand by approximately 23°, presumably to minimize steric interactions with other linkers in the interpenetrated structure. The reason for the different behavior in the Zr and Hf analogues has not been established.

All the functionalized MOFs discussed thus far adopt the typical cubic structure and crystallize with the $Fd\bar{3}m$ symmetry of the parent MOFs; however, close inspection of the PXRD patterns reveals slight differences for MOFs containing L2 (Figure 3a), with additional peaks observed. Single crystals of Zr-L2 (Figure 3b) have both lozenge-shaped and rounded morphologies, unlike the typical well-defined octahedral crystals of the other members of the series. Both of these forms of Zr-L2 crystallize in the lower symmetry orthorhombic $Imma$ space group but have the same connectivity and composition as the

other MOFs, and this is attributed to the presence of different ligand orientations. Of the 12 ligands connected to each Zr₆ cluster, four ligands in an equatorial plane are planar with disordered methyl units (Figure 3c) while the other eight ligands adopt a conformation where the central dimethylphenylene unit is twisted by approximately 40° out of the plane of conjugation, and the methyl groups are fully ordered (Figure 3d). Twisting of the ligands in Zr-L2 is believed to be the result of steric interactions between the bulky methyl groups and adjacent phenyl units of the other interpenetrated net, which are in close proximity (Figure 3e).

It is interesting to note that L4, which contains fluorine atoms in the same positions that L2 contains methyl groups, can be incorporated into Zr and Hf MOFs with the expected cubic symmetry, as the steric interactions imposed by the fluorine atoms are insufficient to drive the structural perturbation observed in Zr-L2. In the crystal structure of Zr-L2 the ligands of one net bow away from the Zr₆ cluster of the second net, while in Zr-L4 and the rest of the MOFs the ligands bow in toward the cluster, and this structural difference is likely to be due to the differing extent of steric interactions (see SI, Section S5).

The PXRD pattern of Zr-L2 changed significantly over the course of N₂ adsorption experiments (Figure 3a). Comparing the experimental PXRD pattern of chloroform exchanged Zr-L2 (Zr-L2 expt) with the predicted pattern from the orthorhombic single crystal structure (Zr-L2 pred), it is clear that some of the peaks match well, while some of them are split, indicating the presence of multiple phases. The PXRD pattern of cubic Zr-L1 was also predicted (Zr-L1 pred), revealing that the experimental pattern of chloroform exchanged Zr-L2 resembles both the orthorhombic and cubic predicted patterns to some extent, again suggesting a mixture of two phases. The presence of mixed phases of Zr-L2 suggests that the material is dynamic and that it may be able to transition from the orthorhombic ($Imma$) to the cubic ($Fd\bar{3}m$) phase by rotation of the central dimethylphenylene units. This is indeed confirmed by PXRD analysis of Zr-L2 after N₂ adsorption experiments (Zr-L2 post-BET) with the pattern now in excellent agreement

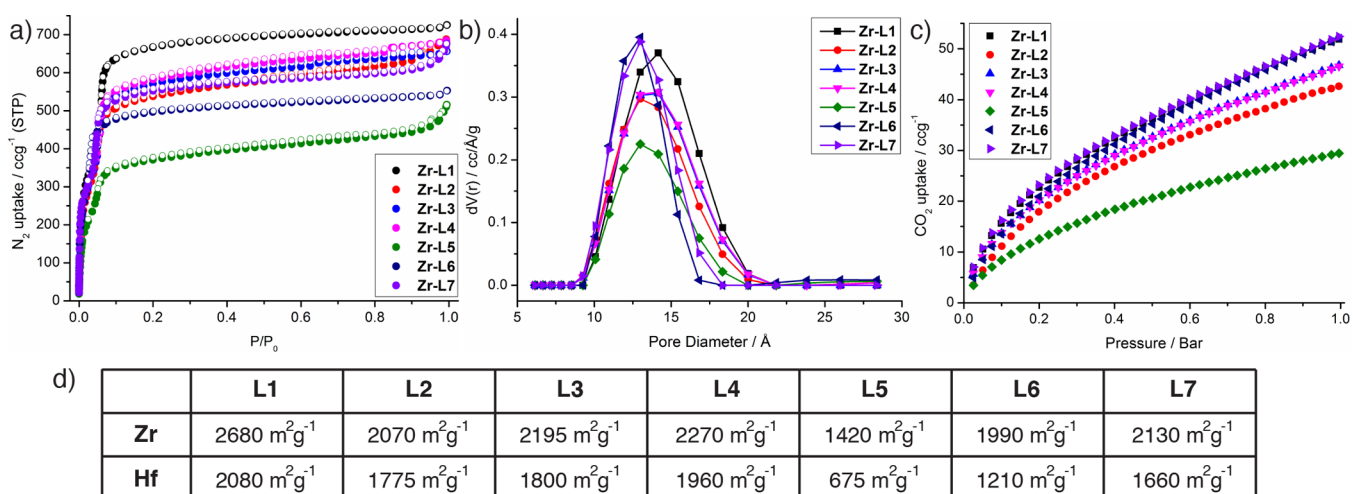


Figure 4. (a) N₂ adsorption and desorption isotherms collected at 77 K for the Zr MOFs. (b) Corresponding pore size distributions (QSDFT) for the MOF series. Analogous data for the Hf MOFs are given in the SI, Section S7. (c) CO₂ adsorption isotherms (273 K) of the Zr MOFs. (d) Calculated BET surface areas for all 14 Zr and Hf MOFs.

with the predicted pattern for cubic **Zr-L1**. Prior to N₂ uptake experiments the material was activated by heating at 120 °C for 20 h, and we believe that, upon heating, the ligands rotate to adopt the linear geometry found in the cubic MOFs. We further investigated this phenomenon by performing variable-temperature PXRD, and the same trend was observed, confirming that heating results in a structural modification and crystallographic phase change (see SI, Section S5).

With the series of interpenetrated Zr and Hf MOFs in hand, we decided to analyze and compare the effect of substitution on their physical properties. From the thermogravimetric analysis (TGA) profiles (see SI, Section S6) it is clear that the thermal stabilities of the materials are relatively unaffected by the presence of either Zr₆ or Hf₆ clusters with degradation occurring at approximately the same temperature. TGA experiments were performed under an air atmosphere, resulting in decomposition of the MOFs to either ZrO₂ or HfO₂, and the increased mass of Hf relative to Zr accounts for the smaller percentage mass losses that are observed for the Hf MOFs. Ligand functionalization results in slightly altered thermal properties; however, there is no obvious negative impact on the MOFs' thermal stabilities, with all 14 materials decomposing at ~450–500 °C.

Comparing the N₂ uptakes of the Zr MOFs (see SI, Section S7, and Figure 4a) it is evident that ligand functionalization results in a reduction in gravimetric N₂ uptake compared with **Zr-L1**, as would be expected. The N₂ uptakes of **Zr-L2**, **Zr-L3**, and **Zr-L4** are similar, which is reassuring as all three MOFs contain two pendant moieties of similar mass: either methyl groups or fluorine atoms. The porosity of **Zr-L7** is similar to those of the MOFs containing pendant dimethyl/fluorine moieties, while **Zr-L6** displays a slightly lower uptake. The reason for the lower than expected BET surface area of **Zr-L5** (1420 m² g⁻¹) is not immediately obvious; however, low values were consistently observed for multiple batches. It should be noted that the uptake of **Hf-L5** (675 m² g⁻¹) is also lower than expected, and therefore it may be plausible that the activation conditions were ineffective for MOFs containing **L5** or that during activation the MOFs were partially collapsing. The calculated pore-size distributions (QSDFT) are consistent with the functional groups occupying the pore space of the MOFs, with an observed reduction of the main pore diameter from

14.2 Å in **Zr-L1** to 13.0 Å in **Zr-L7** (Figure 4b). Similar trends were observed for the Hf MOFs. CO₂ uptake isotherms of the Zr MOFs were collected at 0 °C (see SI, Section S7) to examine the potential for MOF-guest interactions and reveal that, while ligand functionalization does not significantly improve the CO₂ uptake capacities under the pressure range investigated (Figure 4c), the similar uptakes obtained for **Zr-L1**, **Zr-L6**, and **Zr-L7** (they are superimposed in Figure 4c) suggest that naphthyl and benzothiadiazolyl units do enhance CO₂ uptake to some extent. This enhancement comes in spite of the incorporation of bulky aromatics/heterocycles, presumably through favorable interactions between CO₂ and either the π -system of **Zr-L6** or the electron-rich heterocycle of **Zr-L7**, which has been observed previously in a related Cu-MOF.⁶³

Given that **L1-Me**₂ and its derivatives exhibit interesting absorption properties, and with the incorporation of known chromophores such as naphthyl^{64,65} and benzothiadiazolyl^{66,67} units into the MOFs, solid-state (SS) UV–vis spectra of all the **Zr-Ln** MOFs were collected (Figure 5a) and compared with those of the dimethyl esters (the diesters are a better model for the Zr MOFs as hydrogen bonding between carboxylates is nullified) and free acids of the ligands (see SI, Section S8). The comparisons revealed that in most cases the spectroscopic

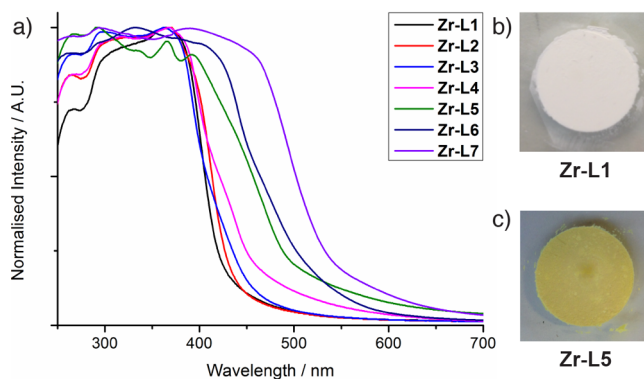


Figure 5. (a) Comparison of the SS-UV–vis spectra of the Zr MOFs. Photographs of (b) **Zr-L1** and (c) **Zr-L5** highlight the unexpected intense yellow color of **Zr-L5**.

properties of the MOFs are generally inherited from the respective ligand.

In particular, it is clear that the benzothiadiazolyl containing MOF (**Zr-L7**; a deep yellow solid) absorbs furthest into the visible region (~ 600 nm), with its strongest absorbance occurring at $\lambda_{\text{max}} = 391$ nm. **Zr-L6**, a pale yellow solid comprised of naphthyl chromophores, also absorbs well into the visible region ($\lambda_{\text{max}} = 333$ nm), aligning well with the absorption properties of **L6-Me₂**. Similarly, **Zr-L5** absorbs in the visible region and is yellow (Figure 5c), correlating well with the SS-UV-vis spectra, despite **L5-H₂** and **L5-Me₂** being white. The red-shifted absorption of **Zr-L5** relative to that of **L5-Me₂** can be ascribed to an LMCT transition that appears as a shoulder at approximately 460 nm.⁶⁸ These transitions have been well described for both Zr^{IV}- and Ti^{IV}-based UiO-66 systems,⁶⁹ and here they are further red-shifted due to the high degree of conjugation within these peb^{2-} ligand systems. More generally, the transitions would be more appropriately described as ligand-to-cluster charge transfer (LCCT) since any participation in the CT comes from a cumulative cluster-centered energy state.⁷⁰

The SS-UV-vis absorption features of the MOFs and the conjugated nature of their bridging ligands prompted us to examine their respective emission behavior (see SI, Section S9) by solid-state photoluminescence spectroscopy in the presence of different small-molecule analytes to determine their potential for sensing. Emission spectra were collected for dry and wetted ligands, diesters, and MOFs, as well as MOF samples in the presence of gaseous N₂, CO₂, and H₂S. Small shifts in emission maxima were observed when the MOFs were exposed to various gases, although the most significant changes occurred upon wetting (see SI, Figure S34), which was not evident for the diesters (see SI, Figure S33). For example, **Zr-L1** shows a demonstrable red-shift upon exposure to a hydrated environment, with $\lambda_{\text{em}} = 407$ nm drifting to 423 nm, and Φ_{F} decreasing from 0.17 to 0.12 (Figure 6a).

We see no such effects with **Zr-L5**, where the central aryl-moiety of **L5** is decorated with four fluorine atoms. The emission profiles are almost identical under both dry and wet conditions with little impact upon Φ_{F} (Figure 6b). Having pores lined with fluorine atoms, we posit that the fluorescence emission of **Zr-L5** does not change under hydrating conditions

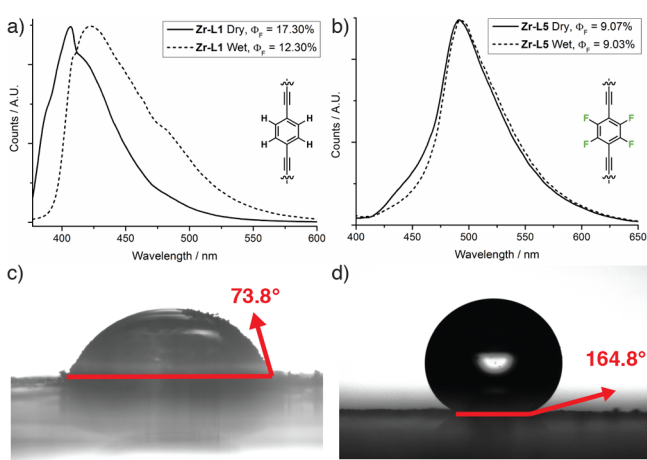


Figure 6. Normalized solid-state photoluminescence emission profiles of (a) **Zr-L1** and (b) **Zr-L5**, under dry and wet conditions. Contact angles were measured for (c) **Zr-L1** and (d) **Zr-L5**.

due to the increased hydrophobicity of the material, preventing water from penetrating into and interacting with the framework. Contact angles of packed powdered samples of **Zr-L1** and **Zr-L5** were measured to understand whether differences in hydrophobicity are responsible for the different emission behaviors (Figure 6c,d, and SI, Section 10). **Zr-L1** has a contact angle of $\sim 73.8^\circ$ indicative of a hydrophilic material, while **Zr-L5** has a contact angle of $\sim 164.8^\circ$ which is typical of superhydrophobic materials.⁷¹

These measurements show that small changes to the bridging organic ligand can considerably alter the MOF's hydrophobicity.⁷² Recently, in a report by Maji et al., a self-cleaning Zn MOF containing alkoxyoctadecyl (C₁₈)-substituted peb^{2-} ligands displayed superhydrophobic behavior,⁷³ while MOFs containing fluorine-abundant ligands have been shown to be hydrophobic.^{74,75} In contrast, we have shown that, by substitution of only one-third of the aromatic protons for fluorine atoms in the organic ligand, one can generate a superhydrophobic surface comparable to the remarkable examples detailed above.^{71–75} **Zr-L5** is an example of a stable, carboxylate-based fluorinated MOF, and we anticipate that other functionalized peb^{2-} ligands could be synthesized and incorporated into interpenetrated Zr MOFs to control hydrophobicity.

Of all the MOFs examined, **Zr-L6** and **Zr-L7** exhibited the most significant changes in the presence of the different analytes likely as a consequence of the intrinsic fluorescence of their functional units. The solid-state fluorescence emission of evacuated **Zr-L7** ($\lambda_{\text{em}} = 500$ nm; $\lambda_{\text{ex}} = 468$ nm, Figure 7) is

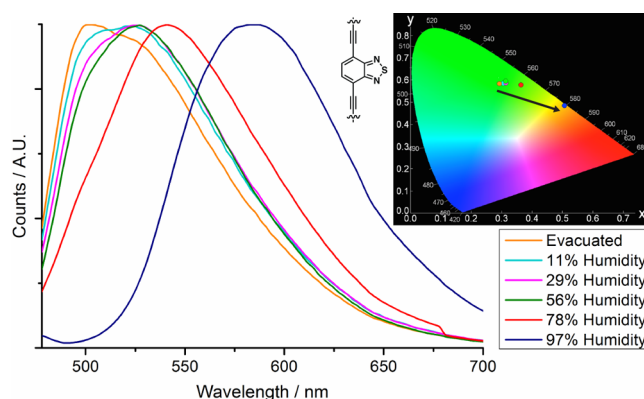


Figure 7. Normalized solid-state photoluminescence spectra of **Zr-L7** upon exposure to differing relative humidity ($\lambda_{\text{ex}} = 468$ nm). Inset: Chromaticity diagram demonstrating dramatic red-shift at 97% humidity.

noticeably different to the corresponding diester **L7-Me₂** ($\lambda_{\text{em}} = 525$ nm; $\lambda_{\text{ex}} = 450$ nm), with a hypsochromic shift in the major emission band due to separation of ligands in the MOF removing any interligand CT, as well as the influence of the more accessible LCCT noted above. More specifically, **Zr-L7** exhibits two clear transitions centered at 500 and 525 nm.

For both MOFs, the most sensitive fluorescence emission change is observed upon hydration, with the pronounced changes in **Zr-L7** suggesting application as a water vapor sensor (Figure 7). As **Zr-L7** is exposed to hydrated environments, the 500 nm emission band begins to quench, while the emission at 525 nm red-shifts to 586 nm (both at 97% relative humidity (H_{rel}) and when wetted, $\lambda_{\text{ex}} = 468$ nm), a significant λ_{max} color shift of 86 nm (see chromaticity in Figure 7 inset). **Zr-L7** also

exhibits the largest response factor ($RF = (\lambda_{\max}/\lambda_0) - 1$, where λ_0 is the emission of dried Zr-L7) for $H_{\text{rel}} = 97\%$ for a Zr-MOF at 0.17.⁵⁴ Particularly noteworthy is the emission shift at H_{rel} levels as low as 11% ($RF = 0.05$) demonstrating the high sensitivity of this material toward water vapor. Of the other MOFs, Zr-L6 shows the most significant changes in emission as humidity increases with a bathochromic shift of λ_{em} from 487 to 521 nm (see SI, Figure S36), while gaseous CO_2 , N_2 , and H_2S cause slight alterations to the fluorescence emission of both Zr-L6 and Zr-L7 (see SI, Figure S34).

We believe that hydration of the nodes,⁷⁶ coupled with the degree of conjugation for Zr-L7 (and Zr-L6) results in the raising of the HOMO levels for the noted LCCT, causing a slight bathochromic shift in the solid-state absorption spectrum (see SI, Figure S38) and a dramatic red-shift in the emission. For Zr-L7 this is further shifted by cooperative hydrogen-bonding effects with L7 (as seen with other protic solvents), compared with Zr-L6 where hydrogen bonding to the naphthyl units is not possible. Few studies have reported intrinsic fluorescence sensing of water by MOFs.^{54,77–79} This is noteworthy since Zr-MOFs are ideal platforms for water sorption³² and sensing applications due to their well-known aqueous stability^{46,80,81} and inherent vacancies made available upon activation from indiscriminately defective Zr-clusters within the networks.^{28,82,83} Indeed, PXRD analysis showed that Zr-L7 was unchanged after the humidity profile was collected (see SI, Figure S39).

In parallel to the emission studies noted above, we examined the photoluminescence spectra of the MOFs in the presence of liquid analytes, with a range of different behaviors observed across the series (see SI, Figure S40). Zr-L2 exhibits the most pronounced solvatochromism of the series, with a modest trend relating to solvent dipole moment (Figure 8, where interacting

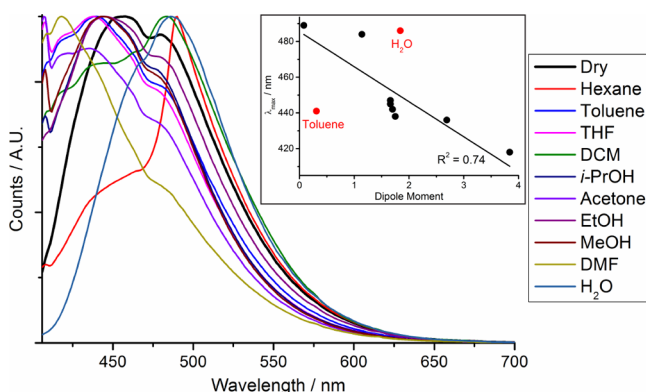


Figure 8. Normalized solid-state photoluminescence emission spectra of Zr-L2 after exposure to various solvents ($\lambda_{\text{ex}} = 396$ nm). Inset: Correlation of change in λ_{max} with solvent dipole moment; water and toluene have been excluded from correlation as they demonstrate direct interaction.

water (node coordination) and toluene (π -stacking) behave as outliers). In contrast, Zr-L7 demonstrates less pronounced solvatochromism, with no distinct trends relating to solvent dipole moment, dielectric, or polarity indices. It is worth noting that L2-Me₂ and L7-Me₂ show no distinctive solvent-dependent emission shifts in the solid state (see SI, Figure S43), in contrast to their respective Zr MOFs. This confirms the requirement of the framework topology for the solvent- and hydration-dependent emission behavior.

Interestingly, Zr-L2 exhibits two radiative transitions in its emission profile (Figure 9), which appear to be inherited from

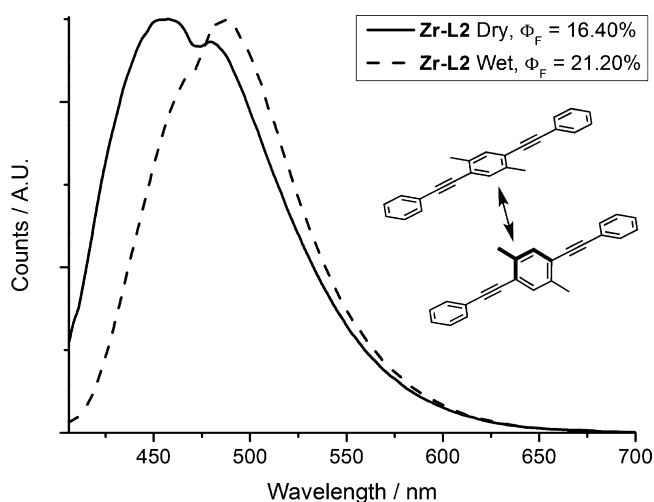


Figure 9. Normalized solid-state photoluminescence emission of Zr-L2 under dry and wet conditions alongside a schematic representation of the observed twisting of the ligands ($\lambda_{\text{ex}} = 396$ nm).

the ligand (see SI, Section 9). We hypothesize that the two radiative transitions are related to differing ligand conformations derived from twisting of the central dimethylphenylene units, as seen in its solid-state structure; twisting of the bridging dimethylphenylene moiety is also present in the crystal structure of L2-Me₂ (see SI, Figure S3). In comparison with the emission spectrum of dried Zr-L2, the intensity of the transition at 465 nm decreases upon wetting. This decrease in intensity suggests that water is causing a structural perturbation of the MOF, presumably by altering the degree of ligand twisting. Furthermore, the decrease in intensity at $\lambda_{\text{em}} = 465$ nm is accompanied by an increase in Φ_{F} , indicative of a higher population of decay centered on the transition at $\lambda_{\text{em}} = 486$ nm. It is worth noting that this observation is purely with material that has been exposed to liquid water; exposure to a range of increasing H_{rel} values perturbs the system only minimally. Coupled with the observed crystallographic transformation from the orthorhombic (twisted/planar ligands) to cubic structure (planar ligands) under heating noted above, these emission data lead us to believe that wetting may result in an increased population of the planar ligand conformation.

From these results, it is clear that solid-state photoluminescence spectroscopy is a versatile tool to not only probe host–guest interactions in MOFs (with potential for sensing) but also physical properties such as hydrophobicity, and subtle structural features such as the ligand rotation phenomenon observed in Zr-L2.

CONCLUSIONS

We have prepared a series of interpenetrated Zr and Hf MOFs comprised of functionalized 4,4'-[1,4-phenylene-bis(ethyne-2,1-diyl)]-dibenzoate ligands and shown that, while functionalization does not affect overall topology, it does induce subtle changes in linker orientation and net-net interactions in the solid state. In particular, the pendant methyl groups of Zr-L2 induce a change in crystal habit and symmetry, through steric clashes and resultant twisting of dimethylphenylene units to form an orthorhombic structure, which can subsequently be

converted to the parent cubic form by heating, with the twisted dimethylphenylene units returning to planarity. The MOFs have excellent porosity, with the introduction of aromatic units and nucleophilic heterocycles enhancing CO₂ uptake. Access to this related series of MOFs with intrinsically fluorescent linkers has allowed us to probe their structures and properties using solid-state photoluminescence spectroscopy, demonstrating the versatility and potential power of the technique. The subtle structural changes described for Zr-L2 can be observed in the relative intensities of different emission maxima when spectra are collected under different conditions. Incorporation of naphthyl and benzothiadiazolyl fluorophores into Zr-L6 and Zr-L7, respectively, generates MOFs that can detect guest molecules, with highly sensitive emission changes upon wetting and structural stability suggesting possible use of Zr-L7 as a water sensor. Additionally, the superhydrophobicity of the partially fluorinated Zr-L5 can be seen by the close correlation between its spectra collected when wet and dry, in contrast to the large shifts seen for the hydrophilic Zr-L1, and these results have been confirmed by contact angle measurements.

The fact that functionalization of the peb^{2-} scaffold induces such structural and physical variety in the resulting MOFs, coupled with the fact that many of the properties are not present in the free ligands, has allowed us to demonstrate not only the potential of the series for simple introduction of versatile functionality into MOFs to enhance their physical properties, but also the potential for using photoluminescence spectroscopy as a facile technique to probe these subtle changes in MOF structure, physical properties, and host–guest interactions. We also expect the dynamic behavior of these interpenetrated Zr and Hf MOFs to modulate their mechanical properties, while studies investigating modulation of their physical and optical properties by synthesizing new functionalized analogues are underway.

■ ASSOCIATED CONTENT

■ Supporting Information

The Supporting Information is available free of charge on the ACS Publications website at DOI: 10.1021/jacs.7b02184.

X-ray crystallographic data for L1-Me2, L2-Me2, L3-Me2, L4-H2, L4-Me2, L5-Me2, Hf-L3, Hf-L4, Hf-L5, Hf-L6, Hf-L7, Zr-L2, Zr-L3, Zr-L4, Zr-L5, Zr-L6, and Zr-L7 (CIF)

Synthesis of all ligands and MOFs, PXRD, TGA, gas adsorption analysis, SS-UV–vis, and photoluminescence spectroscopy (PDF)

■ AUTHOR INFORMATION

Corresponding Authors

*ross.forgan@glasgow.ac.uk

*b.blight@unb.ca

ORCID

Ross J. Marshall: 0000-0001-5756-0306

Ross S. Forgan: 0000-0003-4767-6852

Notes

The authors declare no competing financial interest. The data which underpin this work are available at <http://dx.doi.org/10.5525/gla.researchdata.398>. CCDC 1516193–1516211 contain the supplementary crystallographic data for this paper.

■ ACKNOWLEDGMENTS

R.S.F. thanks the Royal Society for receipt of a University Research Fellowship and the University of Glasgow for funding. The research was supported by EPSRC (EP/L004461/1). B.A.B. thanks the University of Kent for funding and Edinburgh Instruments (Livingston, UK) for in-kind support. Y.K. is a DSTL-funded postgraduate researcher. We thank Mauro Davide Cappelluti and Prof. Duncan Gregory for access to solid-state UV–vis facilities, Rigaku OD for single-crystal data collection of Zr-L2, and the EPSRC UK National Crystallographic Service for single-crystal data collection.⁸⁴

■ REFERENCES

- (1) Hoskins, B. F.; Robson, R. *J. Am. Chem. Soc.* **1990**, *112*, 1546.
- (2) Kondo, M.; Yoshitomi, T.; Matsuzaka, H.; Kitagawa, S.; Seki, K. *Angew. Chem., Int. Ed. Engl.* **1997**, *36*, 1725.
- (3) Chui, S. S.-Y.; Lo, S. M.-F.; Charmant, J. P. H.; Orpen, A. G.; Williams, I. D. *Science* **1999**, *283*, 1148.
- (4) Li, H.; Eddaoudi, M.; O’Keeffe, M.; Yaghi, O. M. *Nature* **1999**, *402*, 276.
- (5) Seo, J. S.; Whang, D.; Lee, H.; Jun, S. I.; Oh, J.; Jeon, Y. J.; Kim, K. *Nature* **2000**, *404*, 982.
- (6) Long, J. R.; Yaghi, O. M. *Chem. Soc. Rev.* **2009**, *38*, 1213.
- (7) Zhou, H.-C.; Long, J. R.; Yaghi, O. M. *Chem. Rev.* **2012**, *112*, 673.
- (8) Yaghi, O. M.; O’Keeffe, M.; Ockwig, N. W.; Chae, H. K.; Eddaoudi, M.; Kim, J. *Nature* **2003**, *423*, 705.
- (9) Kitagawa, S.; Kitaura, R.; Noro, S.-I. *Angew. Chem., Int. Ed.* **2004**, *43*, 2334.
- (10) Lu, W.; Wei, Z.; Gu, Z.-Y.; Liu, T.-F.; Park, J.; Park, J.; Tian, J.; Zhang, M.; Zhang, Q.; Gentle, T.; Bosch, M.; Zhou, H.-C. *Chem. Soc. Rev.* **2014**, *43*, 5561.
- (11) He, Y.; Zhou, W.; Qian, G.; Chen, B. *Chem. Soc. Rev.* **2014**, *43*, 5657.
- (12) Murray, L. J.; Dinca, M.; Long, J. R. *Chem. Soc. Rev.* **2009**, *38*, 1294.
- (13) Tranchemontagne, D. J.; Park, K. S.; Furukawa, H.; Eckert, J.; Knobler, C. B.; Yaghi, O. M. *J. Phys. Chem. C* **2012**, *116*, 13143.
- (14) Li, J.-R.; Kuppler, R. J.; Zhou, H.-C. *Chem. Soc. Rev.* **2009**, *38*, 1477.
- (15) Sumida, K.; Rogow, D. L.; Mason, J. A.; McDonald, T. M.; Bloch, E. D.; Herm, Z. R.; Bae, T.-H.; Long, J. R. *Chem. Rev.* **2012**, *112*, 724.
- (16) Zhang, Z.; Zhao, Y.; Gong, Q.; Li, Z.; Li, J. *Chem. Commun.* **2013**, *49*, 653.
- (17) Lee, J.; Farha, O. K.; Roberts, J.; Scheidt, K. A.; Nguyen, S. T.; Hupp, J. T. *Chem. Soc. Rev.* **2009**, *38*, 1450.
- (18) Yoon, M.; Srirambalaji, R.; Kim, K. *Chem. Rev.* **2012**, *112*, 1196.
- (19) Liu, J.; Chen, L.; Cui, H.; Zhang, J.; Zhang, L.; Su, C.-Y. *Chem. Soc. Rev.* **2014**, *43*, 6011.
- (20) Cui, Y.; Yue, Y.; Qian, G.; Chen, B. *Chem. Rev.* **2012**, *112*, 1126.
- (21) Kreno, L. E.; Leong, K.; Farha, O. K.; Allendorf, M.; Van Duyne, R. P.; Hupp, J. T. *Chem. Rev.* **2012**, *112*, 1105.
- (22) Hu, Z.; Deibert, B. J.; Li, J. *Chem. Soc. Rev.* **2014**, *43*, 5815.
- (23) Horcajada, P.; Serre, C.; Vallet-Regí, M.; Sebban, M.; Tauler, F.; Férey, G. *Angew. Chem., Int. Ed.* **2006**, *45*, 5974.
- (24) McKinlay, A. C.; Morris, R. E.; Horcajada, P.; Férey, G.; Gref, R.; Couvreur, P.; Serre, C. *Angew. Chem., Int. Ed.* **2010**, *49*, 6260.
- (25) Della Rocca, J.; Liu, D.; Lin, W. *Acc. Chem. Res.* **2011**, *44*, 957.
- (26) Orellana-Tavra, C.; Baxter, E. F.; Tian, T.; Bennett, T. D.; Slater, N. K. H.; Cheetham, A. K.; Fairen-Jimenez, D. *Chem. Commun.* **2015**, *51*, 13878.
- (27) Cavka, J. H.; Jakobsen, S.; Olsbye, U.; Guillou, N.; Lamberti, C.; Bordiga, S.; Lillerud, K. P. *J. Am. Chem. Soc.* **2008**, *130*, 13850.
- (28) Cliffe, M. J.; Wan, W.; Zou, X.; Chater, P. A.; Kleppe, A. K.; Tucker, M. G.; Wilhelm, H.; Funnell, N. P.; Coudert, F.-X.; Goodwin, A. L. *Nat. Commun.* **2014**, *5*, 4176.

- (29) Feng, D.; Jiang, H.-L.; Chen, Y.-P.; Gu, Z.-Y.; Wei, Z.; Zhou, H.-C. *Inorg. Chem.* **2013**, *52*, 12661.
- (30) Valenzano, L.; Civalleri, B.; Chavan, S.; Bordiga, S.; Nilsen, M. H.; Jakobsen, S.; Lillerud, K. P.; Lamberti, C. *Chem. Mater.* **2011**, *23*, 1700.
- (31) Bai, Y.; Dou, Y.; Xie, L.-H.; Rutledge, W.; Li, J.-R.; Zhou, H.-C. *Chem. Soc. Rev.* **2016**, *45*, 2327.
- (32) Furukawa, H.; Gándara, F.; Zhang, Y.-B.; Jiang, J.; Queen, W. L.; Hudson, M. R.; Yaghi, O. M. *J. Am. Chem. Soc.* **2014**, *136*, 4369.
- (33) Ma, J.; Wong-Foy, A. G.; Matzger, A. J. *Inorg. Chem.* **2015**, *54*, 4591.
- (34) Wang, R.; Wang, Z.; Xu, Y.; Dai, F.; Zhang, L.; Sun, D. *Inorg. Chem.* **2014**, *53*, 7086.
- (35) Feng, D.; Gu, Z.-Y.; Li, J.-R.; Jiang, H.-L.; Wei, Z.; Zhou, H.-C. *Angew. Chem., Int. Ed.* **2012**, *51*, 10307.
- (36) Morris, W.; Voloskiy, B.; Demir, S.; Gándara, F.; McGrier, P. L.; Furukawa, H.; Cascio, D.; Stoddart, J. F.; Yaghi, O. M. *Inorg. Chem.* **2012**, *51*, 6443.
- (37) Mondloch, J. E.; Bury, W.; Fairen-Jimenez, D.; Kwon, S.; DeMarco, E. J.; Weston, M. H.; Sarjeant, A. A.; Nguyen, S. T.; Stair, P. C.; Snurr, R. Q.; Farha, O. K.; Hupp, J. T. *J. Am. Chem. Soc.* **2013**, *135*, 10294.
- (38) Schaate, A.; Roy, P.; Preuße, T.; Lohmeier, S. J.; Godt, A.; Behrens, P. *Chem. Eur. J.* **2011**, *17*, 9320.
- (39) Lippke, J.; Brosent, B.; von Zons, T.; Virmani, E.; Lilienthal, S.; Preuße, T.; Hülsmann, M.; Schneider, A. M.; Wuttke, S.; Behrens, P.; Godt, A. *Inorg. Chem.* **2017**, *56*, 748.
- (40) Chen, D.; Xing, H.; Wang, C.; Su, Z. *J. Mater. Chem. A* **2016**, *4*, 2657.
- (41) Roy, P.; Schaate, A.; Behrens, P.; Godt, A. *Chem. Eur. J.* **2012**, *18*, 6979.
- (42) Doan, T. L. H.; Nguyen, H. L.; Pham, H. Q.; Pham-Tran, N.-N.; Le, T. N.; Cordova, K. E. *Chem. Asian J.* **2015**, *10*, 2660.
- (43) Doan, T. L. H.; Dao, T. Q.; Tran, H. N.; Tran, P. H.; Le, T. N. *Dalton Trans.* **2016**, *45*, 7875.
- (44) Babarao, R.; Rubio-Martinez, M.; Hill, M. R.; Thornton, A. W. *J. Phys. Chem. C* **2016**, *120*, 13013.
- (45) Marshall, R. J.; Griffin, S. L.; Wilson, C.; Forgan, R. S. *J. Am. Chem. Soc.* **2015**, *137*, 9527.
- (46) Marshall, R. J.; Griffin, S. L.; Wilson, C.; Forgan, R. S. *Chem. Eur. J.* **2016**, *22*, 4870.
- (47) Hobday, C. L.; Marshall, R. J.; Murphie, C. F.; Sotelo, J.; Richards, T.; Allan, D. R.; Düren, T.; Coudert, F.-X.; Forgan, R. S.; Morrison, C. A.; Moggach, S. A.; Bennett, T. D. *Angew. Chem., Int. Ed.* **2016**, *55*, 2401.
- (48) Marshall, R. J.; Richards, T.; Hobday, C. L.; Murphie, C. F.; Wilson, C.; Moggach, S. A.; Bennett, T. D.; Forgan, R. S. *Dalton Trans.* **2016**, *45*, 4132.
- (49) Fasina, T. M.; Collings, J. C.; Burke, J. M.; Batsanov, A. S.; Ward, R. M.; Albesa-Jove, D.; Porres, L.; Beeby, A.; Howard, J. A. K.; Scott, A. J.; Clegg, W.; Watt, S. W.; Viney, C.; Marder, T. B. *J. Mater. Chem.* **2005**, *15*, 690.
- (50) Carboni, M.; Lin, Z.; Abney, C. W.; Zhang, T.; Lin, W. *Chem. Eur. J.* **2014**, *20*, 14965.
- (51) Nagarkar, S. S.; Desai, A. V.; Ghosh, S. K. *Chem. Commun.* **2014**, *50*, 8915.
- (52) Nagarkar, S. S.; Desai, A. V.; Ghosh, S. K. *Chem. Eur. J.* **2015**, *21*, 9994.
- (53) Desai, A. V.; Samanta, P.; Manna, B.; Ghosh, S. K. *Chem. Commun.* **2015**, *51*, 6111.
- (54) Drache, F.; Bon, V.; Senkowska, I.; Adam, M.; Eychmüller, A.; Kaskel, S. *Eur. J. Inorg. Chem.* **2016**, 4483.
- (55) Wang, B.; Lv, X.-L.; Feng, D.; Xie, L.-H.; Zhang, J.; Li, M.; Xie, Y.; Li, J.-R.; Zhou, H.-C. *J. Am. Chem. Soc.* **2016**, *138*, 6204.
- (56) Jiang, H.-L.; Feng, D.; Wang, K.; Gu, Z.-Y.; Wei, Z.; Chen, Y.-P.; Zhou, H.-C. *J. Am. Chem. Soc.* **2013**, *135*, 13934.
- (57) Aguilera-Sigalat, J.; Bradshaw, D. *Chem. Commun.* **2014**, *50*, 4711.
- (58) Wei, Z.; Gu, Z.-Y.; Arvapally, R. K.; Chen, Y.-P.; McDougald, R. N.; Ivy, J. F.; Yakovenko, A. A.; Feng, D.; Omary, M. A.; Zhou, H.-C. *J. Am. Chem. Soc.* **2014**, *136*, 8269.
- (59) Deria, P.; Yu, J.; Balaraman, R. P.; Mashni, J.; White, S. *Chem. Commun.* **2016**, *52*, 13031.
- (60) Schaate, A.; Roy, P.; Godt, A.; Lippke, J.; Waltz, F.; Wiebcke, M.; Behrens, P. *Chem. Eur. J.* **2011**, *17*, 6643.
- (61) Marshall, R. J.; Hobday, C. L.; Murphie, C. F.; Griffin, S. L.; Morrison, C. A.; Moggach, S. A.; Forgan, R. S. *J. Mater. Chem. A* **2016**, *4*, 6955.
- (62) Gutov, O. V.; Molina, S.; Escudero-Adán, E. C.; Shafir, A. *Chem. Eur. J.* **2016**, *22*, 13582.
- (63) Song, C.; He, Y.; Li, B.; Ling, Y.; Wang, H.; Feng, Y.; Krishna, R.; Chen, B. *Chem. Commun.* **2014**, *50*, 12105.
- (64) Gutierrez Tovar, M.; Cohen, B.; Sanchez, F.; Douhal, A. *Phys. Chem. Chem. Phys.* **2016**, *18*, 27761.
- (65) Mallick, A.; Garai, B.; Addicoat, M. A.; Petkov, P. S.; Heine, T.; Banerjee, R. *Chem. Sci.* **2015**, *6*, 1420.
- (66) Parker, T. C.; Patel, D. G.; Moudgil, K.; Barlow, S.; Risko, C.; Bredas, J.-L.; Reynolds, J. R.; Marder, S. R. *Mater. Horiz.* **2015**, *2*, 22.
- (67) Neto, B. A. D.; Carvalho, P. H. P. R.; Correa, J. R. *Acc. Chem. Res.* **2015**, *48*, 1560.
- (68) Pritchard, V. E.; Thorp-Greenwood, F. L.; Balasingham, R. G.; Williams, C. F.; Kariuki, B. M.; Platts, J. A.; Hallett, A. J.; Coogan, M. P. *Organometallics* **2013**, *32*, 3566.
- (69) Fu, Y.; Sun, D.; Chen, Y.; Huang, R.; Ding, Z.; Fu, X.; Li, Z. *Angew. Chem., Int. Ed.* **2012**, *51*, 3364.
- (70) Horiuchi, Y.; Toyao, T.; Saito, M.; Mochizuki, K.; Iwata, M.; Higashimura, H.; Anpo, M.; Matsuoka, M. *J. Phys. Chem. C* **2012**, *116*, 20848.
- (71) Law, K.-Y. *J. Phys. Chem. Lett.* **2014**, *5*, 686.
- (72) Nguyen, J. G.; Cohen, S. M. *J. Am. Chem. Soc.* **2010**, *132*, 4560.
- (73) Roy, S.; Suresh, V. M.; Maji, T. K. *Chem. Sci.* **2016**, *7*, 2251.
- (74) Chen, T.-H.; Popov, I.; Zenasni, O.; Daugulis, O.; Miljanic, O. S. *Chem. Commun.* **2013**, *49*, 6846.
- (75) Chen, T.-H.; Popov, I.; Kaveevitvichai, W.; Chuang, Y.-C.; Chen, Y.-S.; Jacobson, A. J.; Miljanić, O. Š. *Angew. Chem., Int. Ed.* **2015**, *54*, 13902.
- (76) The hydrogen bonding of water to μ_3 -OH units of $Zr_6O_4(OH)_4$ clusters in related Zr MOFs has been observed crystallographically: Ko, N.; Hong, J.; Sung, S.; Cordova, K. E.; Park, H. J.; Yang, J. K.; Kim, J. *Dalton Trans.* **2015**, *44*, 2047.
- (77) Yu, Y.; Zhang, X.-M.; Ma, J.-P.; Liu, Q.-K.; Wang, P.; Dong, Y.-B. *Chem. Commun.* **2014**, *50*, 1444.
- (78) Douvali, A.; Tsipis, A. C.; Eliseeva, S. V.; Petoud, S.; Papaefstathiou, G. S.; Malliakas, C. D.; Papadas, I.; Armatas, G. S.; Margiolaki, L.; Kanatzidis, M. G.; Lazarides, T.; Manos, M. J. *Angew. Chem., Int. Ed.* **2015**, *54*, 1651.
- (79) Fard, Z. H.; Kalinovsky, Y.; Spasyuk, D. M.; Blight, B. A.; Shimizu, G. K. H. *Chem. Commun.* **2016**, *52*, 12865.
- (80) Liu, X.; Demir, N. K.; Wu, Z.; Li, K. *J. Am. Chem. Soc.* **2015**, *137*, 6999.
- (81) Mondloch, J. E.; Katz, M. J.; Planas, N.; Semrouni, D.; Gagliardi, L.; Hupp, J. T.; Farha, O. K. *Chem. Commun.* **2014**, *50*, 8944.
- (82) Katz, M. J.; Brown, Z. J.; Colon, Y. J.; Siu, P. W.; Scheidt, K. A.; Snurr, R. Q.; Hupp, J. T.; Farha, O. K. *Chem. Commun.* **2013**, *49*, 9449.
- (83) Shearer, G. C.; Chavan, S.; Ethiraj, J.; Vitillo, J. G.; Svelle, S.; Olsbye, U.; Lamberti, C.; Bordiga, S.; Lillerud, K. P. *Chem. Mater.* **2014**, *26*, 4068.
- (84) Coles, S. J.; Gale, P. A. *Chem. Sci.* **2012**, *3*, 683.